DOI: 10.26599/FSHW.2024.9250095

Contents lists available at SciOpen

Food Science and Human Wellness

journal homepage: https://www.sciopen.com/journal/2097-0765

Bifunctional ZrO_2@ZIF-90 nanozyme with high phosphohydrolase activity for sensitive electrochemical detection of methyl parathion

Xiaomin Pang[1], Geoffrey I.N. Waterhouse[2], Ruiqiang Wang[3], Xuguang Qiao[1], Yufeng Sun[1*], Zhixiang Xu[1*]

[1]*Key Laboratory of Food Nutrition and Healthy in Universities of Shandong, College of Food Science and Engineering, Shandong Agricultural University, Tai'an 271018, People's Republic of China*

[2]*School of Chemical Sciences, The University of Auckland, Auckland 1142, New Zealand*

[3]*Shandong Cayon Testing Co., Ltd., Jining, People's Republic of China*

ABSTRACT: In this work, a novel bifunctional zirconium dioxide @ zeolitic imidazolate framework-90 (ZrO_2@ZIF-90) nanozyme was successfully developed for the catalytic degradation and electrochemical detection of methyl parathion (MP). The ZrO_2@ZIF-90 nanozyme with phosphatase hydrolysis activity can convert MP into *p*-nitrophenol (*p*-NP). The addition of ZrO_2 riched in Lewis acid Zr(IV) sites significantly enhanced the phosphatase hydrolysis activity of ZIF-90. ZrO_2@ZIF-90 also displayed satisfactory electrocatalytic performance on account of the high surface area, high porosity and powerful enrichment ability of the ZIF-90 and the excellent ion transfer capacity of ZrO_2. A ZrO_2@ZIF-90 nanozyme modified glassy carbon electrode (ZrO_2@ZIF-90/GCE) was then fabricated to analyze *p*-NP formed through MP degradation. Under the optimized conditions, the developed sensor displayed satisfactory analytical performance with a low limit of detection of 0.53 μmol L^{-1} and two wide linear ranges (3-10 μmol L^{-1} and 10-200 μmol L^{-1}). ZrO_2@ZIF-90 nanozyme accomplished to the degradation and electrochemical detection of MP in river water and spiked fruits. This study identifies a promising new strategy for the design of bifunctional nanozymes for the detection of environmental hazards.

Keywords: Methyl parathion; Organophosphorus pesticides; Nanozyme; ZrO_2@ZIF-90; Electrochemical detection

1. Introduction

Methyl parathion (MP) is a commonly used organophosphorus pesticide in the agricultural and horticultural sectors, offering high efficiency and strong toxicity for control of insect pests[1]. However, MP and its active metabolites act as acetylcholinesterase inhibitors, leading to the accumulation of acetylcholine in peripheral or central nervous system nerve endings, resulting in acute neurotoxicity and respiratory toxicity[2, 3]. Excessive amounts of MP residues in the environment can severely damage ecosystems and threaten human health[4]. Currently, the widely detection methods for MP mainly include high-performance liquid chromatography[5], gas chromatography[6], gas chromatography-mass spectrometry[7],

***Corresponding author**
sunyufeng1208@163.com (Yufeng Sun)
zhixiangxu@sina.com (Zhixiang Xu)

Received 29 June 2023
Received in revised from 23 July 2023
Accepted 20 August 2023

immuno-affinity[8], but these methods exists limitations in practice due to their complex sample processing procedures and expensive equipment. Electrochemical sensors have attracted wide attention with the strength of rapid reaction, high sensitivity and simple operation for detecting MP[9]. To date, the inhibition mechanism of natural biological enzymes have been the majority electrochemical analysis methods for MP, which is susceptible to interference[10]. Harsh condition lead to enzyme deactivation and sensor failure. Thus, finding a material can both degrade and possess high electrocatalytic activity towards MP is essential to reduce its harm to humans and environment.

Nanozymes, novel functional nanomaterials that simulate the catalytic properties of natural enzymes, are attracting increasing interest in various fields such as rapid detection[11, 12]. Nanozymes offer the advantages of better economical, stability, durability, tunable activity and recyclability in contrast to natural enzymes[13]. Metal-organic frameworks (MOFs) are crystalline porous materials, which constructe from metal ions/clusters (nodes) and organic linkers connected by coordination bonds[14, 15]. Owing to their high surface area, ordered porous structures, compositional flexibility and accessible active sites, MOFs are a very promising class of conductive and catalytic material[16-18]. The catalytic activities of MOF materials are closely associated with metal active centers, as well as the functional groups on the linkers. Various MOF-based nanozymes have been developed[19]. To date, most reported MOF-based nanozymes have been designed to offer peroxidase-like or oxidase-like activities, whilst the simulation of organophosphorus hydrolase (OPH) has received little attention.

Zeolitic imidazolate framework-90 (ZIF-90) is a MOF consisted of zinc ions and imidazolate-2-carboxaldehyde (2-ICA) linkers. The composition of ZIF-90 is very similar to the active site in OPH[20], suggesting ZIF-90 may be able to act as a nanozyme with properties similar to OPH. In addition, ZIF-90 possesses the ultrahigh surface area, high porosity and powerful enrichment ability and provide abundant binding sites for target analytes, which is suitable for electrode modification[21]. However, the catalytic efficiency and electrical conductivity of pristine ZIF-90 are modest, requiring compositing with other materials improve the catalytic and conductive properties of ZIF-90 for sensor fabrication.

ZrO_2, a *p*-type oxide semiconductor, has good adsorption capacity and can act as a multifunctional catalyst[22]. And ZrO_2 has a good affinity with phosphorus groups[23, 24]. Furthermore, researches have demonstrated that catalysts with strong Lewis acidity at metal sites are essential for hydrolysis of the phosphonate bond in methyl parathion[25]. In addition, ZrO_2 is widely used in analytical chemistry for sensor development due to its high ionic conductivity[22]. Liu et al developed a carbon black (VXC-72R)/ZrO_2 nanozyme-modified GCE for MP detection in rivers and tea samples[26]. The sensitivity of the electrochemical sensor was greatly improved through ZrO_2 addition to the modified electrode. Meanwhile, nanozyme composites with catalytic activity were designed by some other researches that can degrade pesticides and use electrochemistry to achieve rapid detection of pesticides[27, 28]. Based on the studies described above, we hypothesized that the compositing ZIF-90 and ZrO_2 should create a nanozyme with

good performance for the degradation and electrochemical detection of MP, motivating a detailed investigation.

In this study, a bifunctional ZrO_2@ZIF-90 nanozyme was synthesized then applied to degrade and electrochemically detect MP. As validation of our hypothesis, the ZrO_2@ZIF-90 nanozyme efficiently degraded MP. Further, a ZrO_2@ZIF-90/GCE electrochemical sensor exhibited outstanding analytical performance for MP detection with great anti-interference performance, repeatability and reproducibility. The proposed sensor was successfully implemented in the detection of MP in river water and spiked fruits. To our knowledge, there are few reports on the application of bifunctional nanozymes in the pesticide degradation and electrochemical detection.

2. Experimental Section

2.1 Materials and Chemicals

Detailed information about the materials and chemicals can be found in the Supporting Information.

2.2 Instruments and apparatus

The instruments and apparatus used in this research are described in the Supporting Information.

2.3 Preparation of the ZrO_2@ZIF-90 nanozyme

The ZrO_2@ZIF-90 nanozyme was synthesized using the previous reported method[29]. In brief, a dimethylformamide (DMF) solution of $Zn(CH_3COOH)_2 \cdot 2H_2O$ (0.2 mol L^{-1}, 6 mL), a DMF solution of imidazolate-2-carboxaldehyde (2-ICA) (0.1 mol L^{-1}, 6 mL), and ZrO_2 (3 mg) were mixed and then the resulting mixture vigorously stirred for 5 min. 30 mL of DMF was then added to the mixture to stabilize the as-prepared nanoparticles. The solid product was then obtained by centrifugation at 5595×g for 15 min, then washed with DMF and ethanol (each 4 times). The ZrO_2@ZIF-90 nanozyme was dried under vacuum at room temperature and then stored at 4 ℃ in the dark.The synthesis of the ZrO_2@ZIF-90 nanozyme is shown in Scheme 1a. ZIF-90 was synthesized in the same way as ZrO_2@ZIF-90, but without the addition of ZrO_2.

2.4 Phosphohydrolase activity of ZrO_2@ZIF-90 nanozyme

ZrO_2@ZIF-90 (10.0 mg) was put into 2.0 mL of Tris-HCl buffer solution (50 mmol L^{-1}, pH 9.0) containing MP (0.75 mmol L^{-1}). After incubating for 1.5 h at 80 ℃, the absorbance at 400 nm (corresponding to a MP degradation product) in the solution was recorded (after removal of the catalysts by centrifugation). The catalytic activity of ZIF-90 was determined using the same method. Further, the supernatants were diluted with phosphate buffered saline (PBS, 0.2 mol L^{-1}, pH 7.0) to give a MP concentration around 200 μmol L^{-1} for subsequent electrochemical detection of MP tests.

2.5 Preparation of ZrO_2@ZIF-90/GCE

A GCE was polished to obtain a mirror finish surface ($\Delta Ep \leq 90$ mV), ZrO_2@ZIF-90/GCE was obtained by dropping 8.0 μL the ZrO_2@ZIF-90 suspension (3.0 mg mL^{-1}) on the surface of GCE and drying

in air. Scheme 1b depicts the fabrication process of the ZrO_2@ZIF-90/GCE sensor. The details are shown in Supporting Information.

2.6 Electrochemical measurements

Cyclic voltammograms (CV) and Differential pulse voltammetry (DPV) methods were employed to examine the electrochemical performance of the electrodes with different modification. CV in the MP solutions were scanned over the range -0.2 V to 1.2 V. DPV was also performed from 0.4 V to 1.2 V in the MP solutions.

2.7 Sample preparation

To evaluate the accuracy of the sensor, recovery tests for MP were conducted in apple and pear samples. The concentration of MP in river water and tap water samples were also analyzed using the sensor. The process of sample pretreatment is exhibited in Supporting Information.

3. Results and discussion

3.1 Morphology and structural characterization of ZrO_2@ZIF-90

Scanning electron microscopy (SEM) was used to examine the morphology and particle size of pure ZIF-90 and ZrO_2@ZIF-90. As shown in Fig. 1a and Fig. 1b, ZIF-90 crystallized with a regular three-dimensional granular morphology, and the average particle size was estimated to be ~50 nm[30]. For ZrO_2@ZIF-90 (Fig. 1c), some larger crystal of ZrO_2 could be seen embedded in a matrix of smaller ZIF-90 particles, confirming the successful synthesis of a composite. The energy dispersive spectroscopy (EDS) spectrum of ZrO_2@ZIF-90 confirmed the presence of Zn (6.61 at%), Zr (1.15 at%), N (17.43 at%), C (59.58 at%) and O (15.24 at%) in the composite. The data further supports the successful preparation of a ZrO_2@ZIF-90 composite (Fig. 1d).

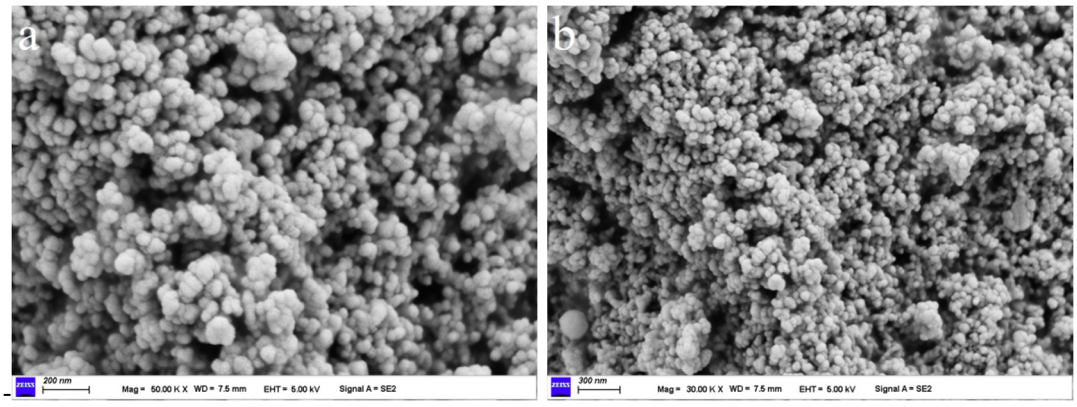

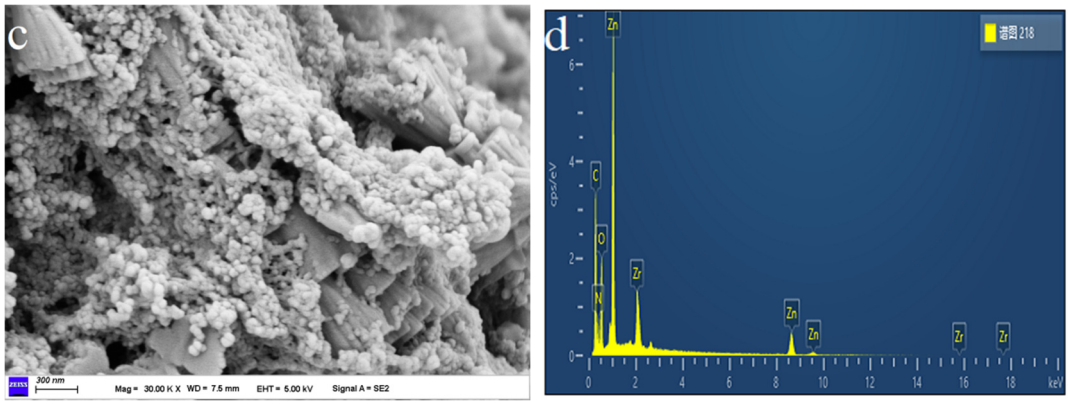

Fig. 1 SEM image of the (a-b) ZIF-90, (c) ZrO_2@ZIF-90, and (d) EDS of ZrO_2@ZIF-90.

Fourier transform infrared (FT-IR) spectroscopy was utilized to study the chemical composition of ZIF-90 and ZrO_2@ZIF-90. Fig. S1a shows the FT-IR spectra for $Zn(CH_3COO)_2.2H_2O$, 2-ICA, ZIF-90 and ZrO_2@ZIF-90. The FT-IR spectrum of $Zn(CH_3COO)_2.2H_2O$ is dominated by broad carboxylate stretching modes in the 1300-1700 cm^{-1} region, with the sharp peak at 694 cm^{-1} being a Zn-O stretching vibration. The 2-ICA linker showed a strong C=O stretching vibration at 1692 cm^{-1}, along with peaks C=N/C-N stretching modes in the 1200-1500 cm^{-1} region. The peak at 792 cm^{-1} is assigned to bending vibrations of the imidazole ring. The FT-IR spectra of ZIF-90 was very similar to that of 2-ICA, with the exception being an additional peak at 537 cm^{-1} which is assigned to a Zn-N stretching vibration in ZIF-90[31-34]. The FT-IR spectrum of ZrO_2@ZIF-90 was similar to that of ZIF-90, with some new weak peaks at 1093 and 454 cm^{-1} ascribe to Zr-O-H bending vibrations (from surface hydroxyl groups) and Zr-O stretching vibrations in ZrO_2, respectively[35, 36].

Powder X-ray diffraction (XRD) patterns were carried out to test the ZIF-90 and ZrO_2@ZIF-90. The XRD pattern of ZIF-90 exhibited characteristic peaks at 12.70°, 15.36°, 17.12°, 22.10° and 26.62° (Fig. S1b), corresponding to the (112), (220), (310), (114) and (134) planes of ZIF-90[37, 38]. For ZrO_2@ZIF-90, additional peaks were seen at 32.05° and 51.20°, which could readily be assigned to the (200) and (222) lattice planes of cubic or tetragonal ZrO_2, respectively[39, 40]. The result further certified the successful synthesis of ZrO_2@ZIF-90 nanozyme.

Next, X-ray photoelectron spectroscopy (XPS) probed the near surface region (top few nanometers) chemical composition of ZIF-90 and ZrO_2@ZIF-90. The full survey spectra for ZIF-90 and ZrO_2@ZIF-90 were shown in Fig. 2a. The survey spectrum of ZIF-90 showed signals due to zinc (Zn 2p ~1021.8 eV), oxygen (O 1s ~ 531.6 eV), nitrogen (N 1s ~399.2 eV) and carbon (C 1s ~284.8 eV). The survey spectrum of ZrO_2@ZIF-90 spectrum showed additional peaks due to Zr (Zr 3d ~181.5 eV), as expected for a composite containing ZrO_2 and ZIF-90. The high resolution N 1s XPS spectra of ZIF-90 and ZrO_2@ZIF-90 is exhibited in Fig. 2b. The spectra show a C-N-Zn peak at 399.2 eV, formed by the interaction of Zn^{2+} with the C=N groups of the 2-ICA linker[41, 42]. A weaker peak at ~401 eV is due to protonated N atoms on the linker (i.e. surface 2-ICA bonded to only 1 Zn^{2+} atom). The C 1s XPS spectrum (Fig. 2c) of ZIF-90 and ZrO_2@ZIF-90 were deconvoluted in three peaks 284.8, 286.0 and 288.4 eV, which are allocated to C=C/C-C, C-N and C=O respectively[43]. Fig. 2d shows the O 1s XPS spectrum of the ZIF-90, the peaks at 531.6, 532.2 and 535.4 eV

were ascribed to C-O, CHO and H_2O groups, respectively[44, 45]. For ZrO_2@ZIF-90, an extra O 1s peak was seen at 529.5 eV due to lattice oxygen in ZrO_2. The Zn 2p XPS spectra for ZIF-90 and ZrO_2@ZIF-90 (Fig. 2e) contained two peaks at 1021.7 and 1044.9 eV in a 2:1 area ration, which could readily be appointed to the Zn $2p_{3/2}$ and Zn $2p_{1/2}$ signals, respectively, of Zn^{2+} in ZIF-90. The Zr 3d spectrum of ZrO_2@ZIF-90 (Fig. 2f) showed two peaks at 181.5 and 183.8 eV in a 3:2 area ratio, typical for the Zr $3d_{5/2}$ and Zr $3d_{3/2}$ signals of Zr^{4+} in ZrO_2. The results further confirm the successful synthesis of a ZrO_2@ZIF-90 nanozyme[46].

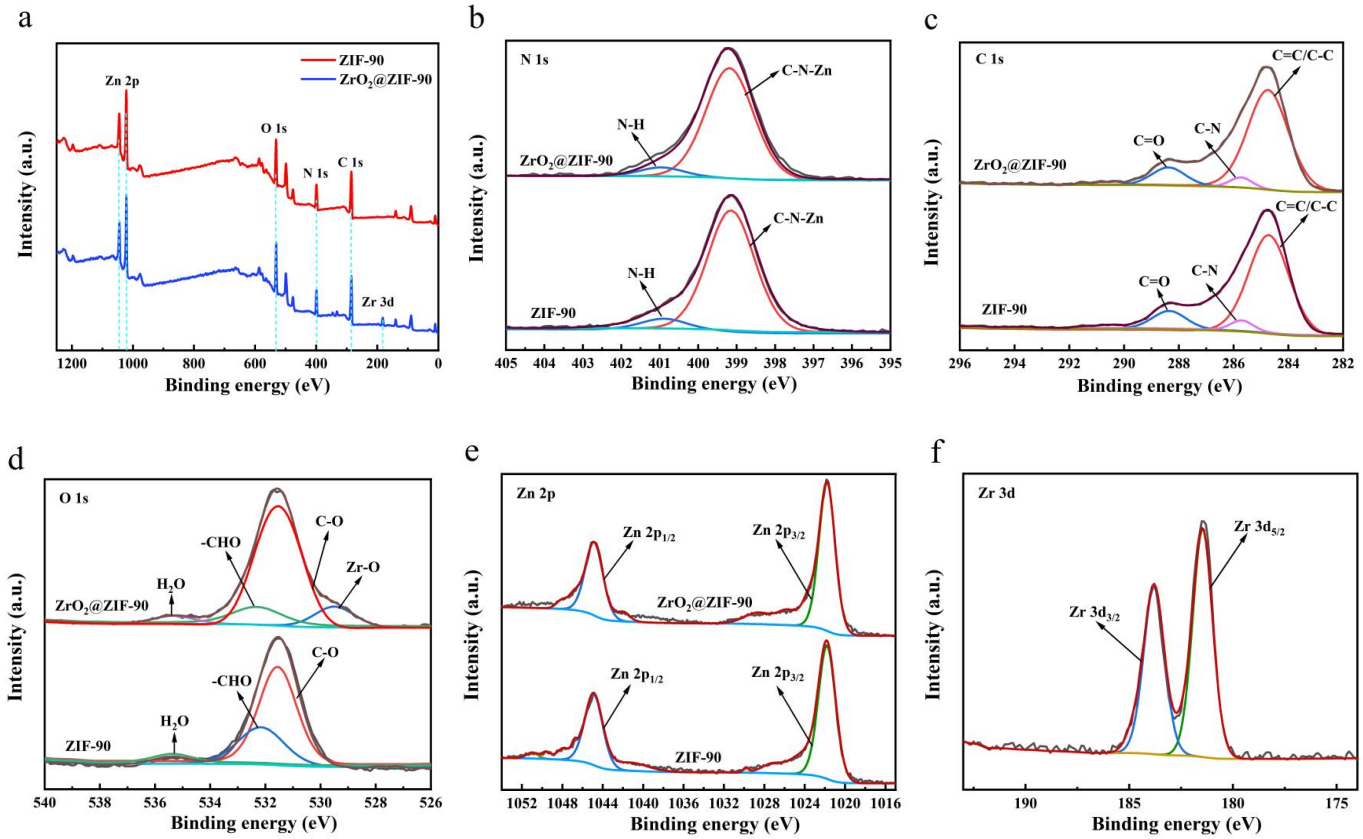

Fig. 2 (a) XPS survey spectra, (b) High-resolution N 1s XPS spectra, (c) High-resolution C 1s spectra, (d) High-resolution O 1s spectra, (e) High-resolution Zn 2p spectra and (f) High-resolution Zr 3d spectra for ZIF-90 and ZrO_2@ZIF-90.

3.2 Phosphohydrolase activity of ZrO_2@ZIF-90 nanozyme

The phosphohydrolase activity of ZIF-90 and the ZrO_2@ZIF-90 nanozyme were investigated, using MP as the reaction substrate. Fig. S2 showed the UV-visible absorption spectra for solutions of MP before and catalysis using ZIF-90 and the ZrO_2@ZIF-90. The photographs in the inset show the colors of the MP solution before and after catalysis. The MP solution were colorless and transparent before catalysis and had a strong absorption peak at 275 nm. After catalysis by ZIF-90 and ZrO_2@ZIF-90, a new absorption peak was appeared at 400 nm whilst the intensity of absorption peak at 275 nm decreased. The solution after catalysis were light yellow, demonstrating ZIF-90 and ZrO_2@ZIF-90 acted as nanozymes and could degrade MP. When ZrO_2@ZIF-90 was used as the catalysts, the degradation of MP was more rapid with the final MP solution being dark yellow[15]. The findings revealed that ZrO_2 enhanced the catalytic activity of ZIF-90 against MP. Negligible MP degradation occurred when MP was incubated with ZrO_2.

In order to design the optimal nanozyme, ZrO_2@ZIF-90 composites were prepared containing different amounts of ZrO_2. Fig. S3 showed that the catalytic activity increased with ZrO_2 addition up to 3.0 mg, then decreased at higher ZrO_2 loadings. The ZrO_2@ZIF-90 nanozyme containing 3.0 mg of ZrO_2 had an activity 1.7 times higher than the pure ZIF-90 nanozyme. The decrease in activity at ZrO_2 loadings above 3.0 mg was likely due to excessive amounts of ZrO_2 covering the active sites of ZIF-90 nanozyme. Therefore, 3.0 mg ZrO_2 was selected as the best loading amount for construction of the ZrO_2@ZIF-90 nanozymes.

The catalytic activity of ZrO_2@ZIF-90 nanozyme towards MP in different kinds of buffer solutions was further investigated. Buffers selected included Britton-Robison (BR), Tris-HCl, Borate-potassium chloride (BA-KCl) and PBS (Fig. 3a). The ZrO_2@ZIF-90 nanozyme possessed the highest catalytic activity for MP degradation in Tris-HCl buffer solution. Fig. 3b showed the effect of pH on the catalytic performance of ZrO_2@ZIF-90. The catalytic activity increased with pH, reaching a maximum at pH 9.0. The observed pH dependence was likely due to the fact that ZIF-90 is unstable and easily decomposed under acidic conditions. The effect of temperature on the performance of the ZrO_2@ZIF-90 nanozyme was explored in the range of 25-90 ℃ (Fig. 3c). As expected, the catalytic activity increased with temperature, reaching a maximum at 80 ℃. Thus 80 ℃ was selected as the optimum catalytic temperature for MP degradation. Fig. 3d explores the effect of catalytic reaction time on MP degradation. The absorbance did not change after reaction for 1.5 h. Accordingly, subsequent MP catalysis experiment were conducted at 80 ℃ for 1.5 h in a Tris-HCl buffer solution.

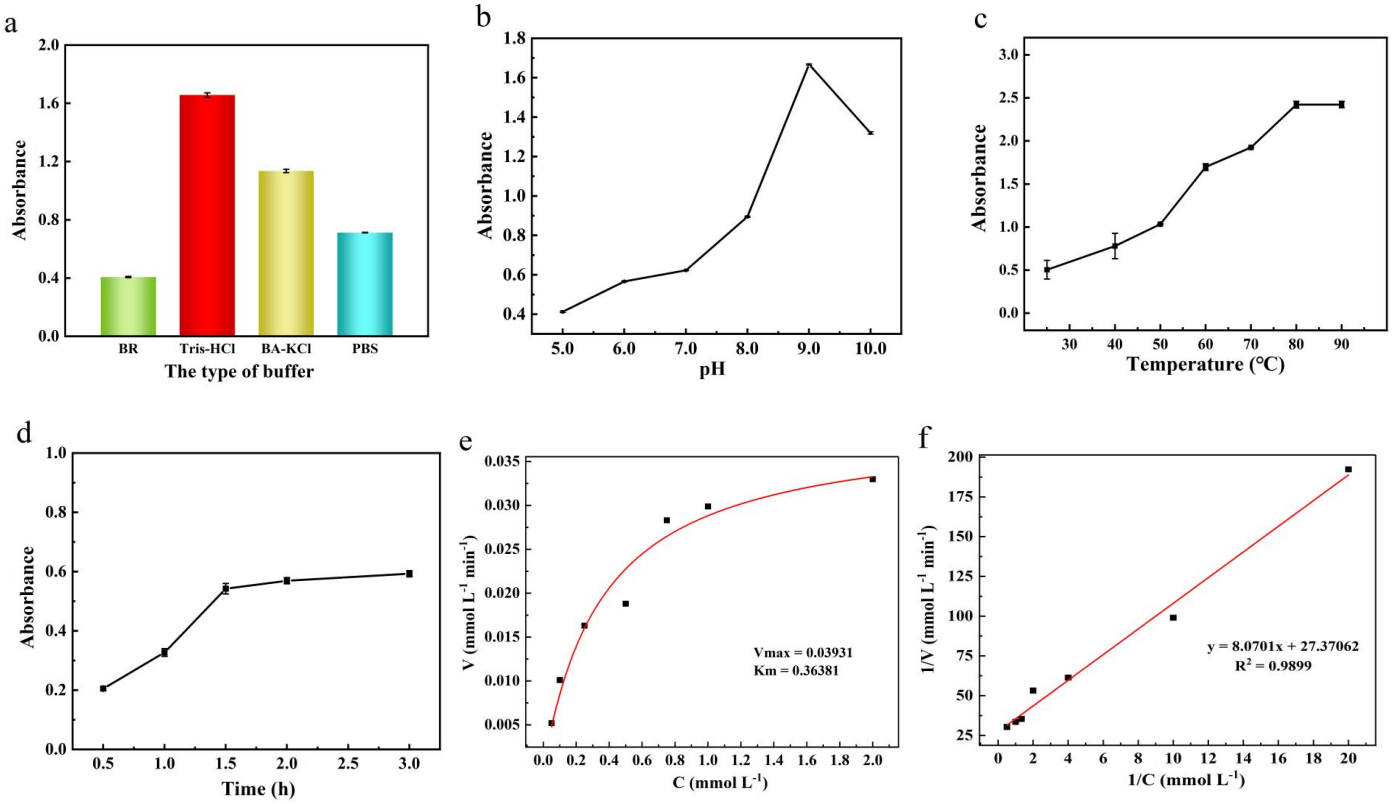

Fig. 3 (a) Catalytic activity of ZrO_2@ZIF-90 for MP degradation in different buffers, (b) Catalytic activity of ZrO_2@ZIF-90 for MP degradation at different pH, (c) Catalytic activity of ZrO_2@ZIF-90 for MP degradation at different temperatures, (d) Catalytic activity of ZrO_2@ZIF-90 for MP degradation at different incubation times. (e) Michaelis-Menten equation curve for hydrolysis of MP catalyzed by ZrO_2@ZIF-90. (f) Lineweaver-Burk plot of the kinetic data of hydrolysis of MP catalyzed by ZrO_2@ZIF-90.

Fig. S4 compares the relative catalytic activity of different dispersion amounts of ZrO_2@ZIF-90 nanozyme for degradation of MP at 80 ℃ over 1.5 h. The ZrO_2@ZIF-90 nanozyme showed the highest catalytic activity when 10.0 mg of ZrO_2@ZIF-90 nanozyme was dispersed in 2 mL of 0.75 mmol/L MP and the concentration of the nanozyme was 5 mg mL^{-1}. At ZrO_2@ZIF-90 amounts above 10.0 mg, the catalyst showed a tendency to aggregate and settle, which might have affected mass transport of MP to active sites. Thus, 10.0 mg ZrO_2@ZIF-90 nanozyme was selected as the optimal addition amount for the catalytic MP degradation reaction.

To further evaluate the phosphohydrolase catalytic performance of the ZrO_2@ZIF-90 nanozyme, steady-state kinetic experiments were conducted based on Michaelis-Menten kinetics (Fig. 3e) and Lineweaver-Burk plot (Fig. 3f), the details of experimental procedure are presented in Supporting Information. The Lineweaver-Burk plot was linear, confirming that the catalytic reaction obeyed Michaelis-Menten kinetics. *Vm* and *Km* values calculated from the plot were 3.9×10^{-2} mmol L^{-1} min^{-1} and 0.36 mmol L^{-1}, respectively. *Km* is a useful indicator of the affinity of an enzyme/nanozyme towards a substrate, with a lower *Km* value representing a higher affinity. As shown in Table S1, the *Km* value for ZrO_2@ZIF-90 was smaller than that of ZIF-90 (1.95 mmol L^{-1}), suggesting that ZrO_2@ZIF-90 possessed a stronger affinity for MP. The higher *Vm* value of ZrO_2@ZIF-90 implied better catalytic efficiency for MP degradation compared to ZIF-90 (2.4×10^{-4} mmol L^{-1} min^{-1}). The results further confirmed that ZrO_2 enhanced the catalytic activity of ZIF-90.

Next, the stability of ZrO_2@ZIF-90 nanozyme was explored. ZrO_2@ZIF-90 retained 73.34% of its initial catalytic activity after five catalytic cycles at 80 ℃ for 1.5 h (Fig. 4a), verifying its recyclability as a nanozyme. Then, the synthesis reproducibility and storage stability of the ZrO_2@ZIF-90 nanozyme were also evaluated. Table S2 showed no significant difference in catalytic activity between different batches of ZrO_2@ZIF-90 nanozyme ($P > 0.05$). Further, ZrO_2@ZIF-90 retained 74.84% of its initial activity after 5 tests spread over 20 days, being stored at room temperature (Fig. 4b). The results indicate ZrO_2@ZIF-90 possessed excellent batch-to-batch reproducibility, together with good recyclability and storage properties.

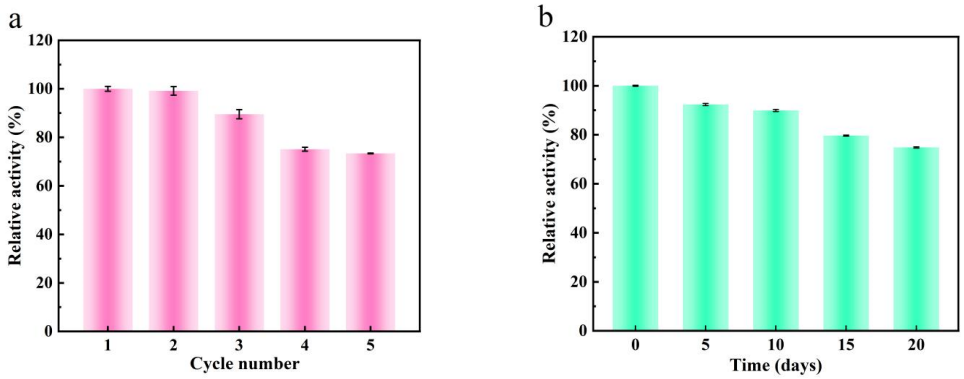

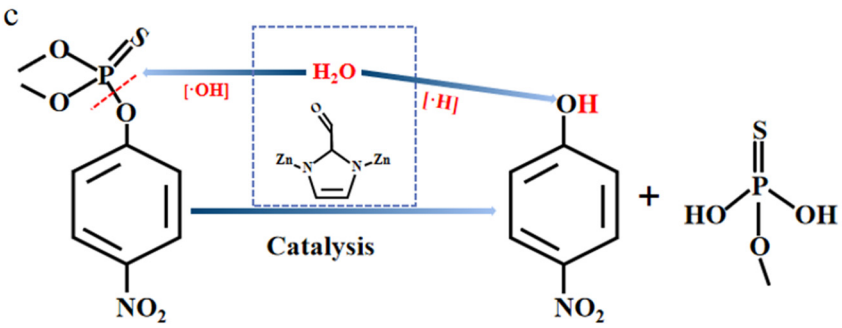

Fig. 4 (a) Reusability of ZrO_2@ZIF-90 nanozyme, (b) Storage stability of ZrO_2@ZIF-90 nanozyme. (c) Molecular structure of ZIF-90 and MP, and the catalytic mechanism for MP degradation over the ZrO_2@ZIF-90 nanozyme.

3.3 Catalytic mechanism of ZrO_2@ZIF-90 nanozyme

The catalytic mechanism of the ZrO_2@ZIF-90 nanozyme for MP degradation was explored by UV-absorption spectroscopy and electrochemical tests. As shown in Fig. S2, after MP was catalytically degraded by the ZrO_2@ZIF-90 nanozyme, a new absorption peak appeared at 400 nm in the UV absorption spectrum whilst the peak at 275 nm associated with MP was attenuated, which indicates that a new substance was formed through the catalytic action of the ZrO_2@ZIF-90 nanozyme on MP. Fig. S5 shows CV curves for a GCE and ZrO_2@ZIF-90/GCE in a MP solution, with the inset showing the proposed electrocatalytic mechanism. For ZrO_2@ZIF-90/GCE, an obvious oxidation peak at +0.94 V is ascribed to the oxidation of para nitrophenol (*p*-NP)[27]. This indicated that the ZrO_2@ZIF-90 nanozyme degraded MP to *p*-NP. We hypothesize that water molecules interact with ZrO_2@ZIF-90 at Zn^{2+} sites, creating ·OH and ·H radicals which attack the P-O bonds of MP, producing *p*-NP and phosphorothioate[47]. The hydrolysis process is shown in Fig. 4c. Furthermore, ZrO_2 was used to improve the catalytic activity of ZIF-90 nanozyme, which was generally attributed to the existence of acidic surface active sites in ZrO_2, including surface oxygen defects. In particular ZrO_2 has Lewis acid sites to activate the P-O bond and make it more susceptible to nucleophilic attack, thus accelerating hydrolysis of MP and improving the catalytic activity[48]. The strongly affinity between ZrO_2 and phosphorus groups was important for enhancing catalytic activity of ZrO_2@ZIF-90 nanozyme for MP degradation to *p*-NP.

3.4 Electrochemical characterization of different electrodes

Electrochemical behavior of the GCE and ZrO_2@ZIF-90/GCE electrodes was investigated by Cyclic voltammetry (CV) in a 200 μmol L^{-1} MP solution (Fig. S5). An irreversible peak appeared at +0.941 V for GCE, and the peak was ascribed to the oxidation of *p*-NP[49]. After the GCE was modified with ZrO_2@ZIF-90, the oxidation peak transferred to more positive potentials (+0.957 V) as the peak current increased. The results indicate that ZrO_2@ZIF-90/GCE had superior electrocatalytic performance than GCE. DPV measurements were employed to explore the electrochemical response of the electrodes with different modification in a 200 μmol L^{-1} MP solution (Fig. 5a). The peak potential (Ep) of the GCE was obtained at +0.764 V and the peak current was 2.859 μA. For ZIF-90/GCE, the peak potential moved towards more positive potentials (+0.884 V) with a concomitant growth in peak current (4.461 μA), which was explained by the ultrahigh surface area,

high porosity and enrichment ability of ZIF-90 and its excellent electrocatalytic properties. The peak intensity reached 5.016 μA after modified with ZrO_2, owing to ion exchange capacity of ZrO_2. Peak current (7.469 μA) of ZrO_2@ZIF-90/GCE was 2.6-fold higher than that of the GCE. It turned out that the ZrO_2@ZIF-90/GCE electrode possessed excellent electrocatalytic performance and good conductivity, thus improving the sensitivity of electrochemical sensor.

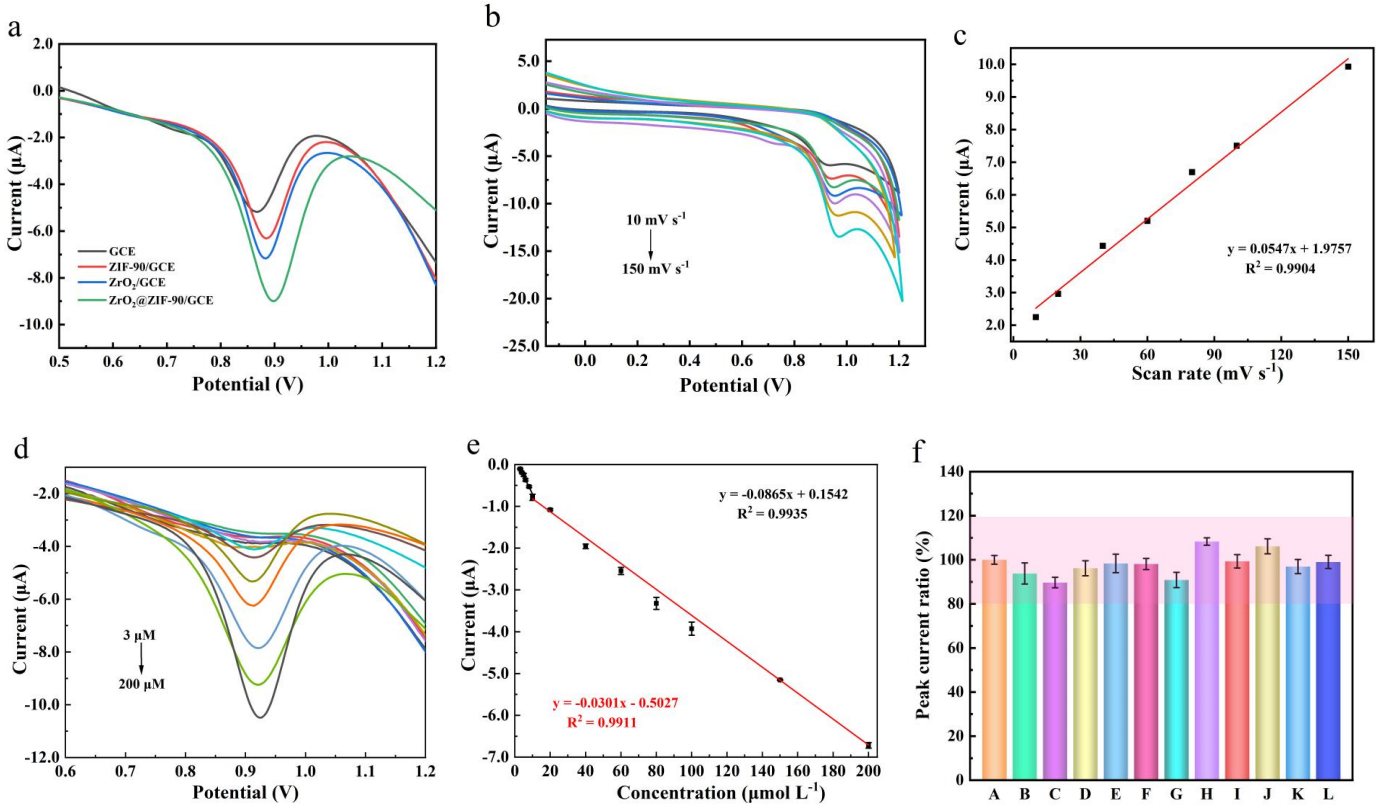

Fig. 5 (a) DPV curves for GCE, ZIF-90/GCE, ZrO_2/GCE and ZrO_2@ZIF-90/GCE in a 200 μmol L^{-1} MP solution in PBS (pH 7.0). (b) CV responses for ZrO_2@ZIF-90/GCE in a 200 μmol L^{-1} MP solution at different scan rates from 10 to 150 mV s^{-1}. (c) Corresponding calibration curve of CV response of ZrO_2@ZIF-90/GCE in a 200 μmol L^{-1} MP solution at different scan rates from 10 to 150 mV s^{-1}. (d) DPV responses of the ZrO_2@ZIF-90/GCE sensor in MP solutions of different concentration. (e) Linear relationship between the peak current and the concentration of MP from 3-10 μmol L^{-1} (black line) and 10-200 μmol L^{-1} (red line). (f) DPV responses of ZrO_2@ZIF-90/GCE towards a 150 μmol L^{-1} MP solution in (A) the absence of interferants, and presence of a 100-fold higher concentration of (B) Cl^-, (C) K^+, (D) Na^+, or (E) NO_2^-; a 10-fold higher concentration of (F) glucose, (G) malathion, (H) glyphosate, (I) chlorpyrifos, (J) acephate, (K) 4-Nitrobenzoic acid and (L) coexistence of all the above interfering substances.

CV curves on ZrO_2@ZIF-90 was acquired at different scanning rates from 10 to 150 mV s^{-1} to explore the control process of *p*-NP oxidation on modified electrodes. A strong linear correlation between oxidation peak currents and the scan rates were found (Fig. 5b). Fig. 5c showed that the fitted equation was Ip = 0.0547v+1.9757 (R^2=0.9904), implying that the oxidation of *p*-NP classified as adsorption controlled electrochemical process[27].

3.5 Optimization of electrochemical detection parameters

In order to further enhance the sensitivity of ZrO_2@ZIF-90 sensor, a series of experimental parameters including the type of electrolyte, pH of the electrolyte, incubation time, the concentration of ZrO_2@ZIF-90 and the volume of ZrO_2@ZIF-90 dispersion were all optimized.

Fig. S6a shows the effect of different electrolyte on the peak current. The maximum peak current was obtained in a PBS (0.2 mol L^{-1}, pH 7.0). Therefore, a PBS was selected for the further experiments.

The oxidation of the analytes and electron transfer were impacted by the pH of the electrolyte. Fig. S6b showed the change of peak current at different pH. The peak current varies with pH from 5.0 to 9.0, and the best peak current is presented at pH = 5.0. This may be due to the fact that phenoxy ions formed by phenol dissociation are not conducive to the formation of phenoxy free radicals under alkaline conditions[50].

Fig. S6c shown the influence of incubation time for electrochemical performance. The peak current appeared a maximum value at incubation of 4.0 min then plateaued. The reaction between ZrO_2@ZIF-90 and *p*-NP was clearly not complete at times shorter than 4.0 min. Accordingly, 4.0 min was the optimal incubation time for further studies.

The concentration and volume of the ZrO_2@ZIF-90 dispersion also influenced the sensitivity of the sensor. From Fig. S6d and Fig. S6e, the peak currents increased initially and then decreased with the amount of ZrO_2@ZIF-90, reaching the maximum value at 3.0 mg mL^{-1} and 8.0 μL, respectively. Excess of ZrO_2@ZIF-90 on the electrode surface resulted in a slower rate of electron transfer. Consequently, dispersion concentrations and volumes of 3.0 mg mL^{-1} and 8.0 μL, respectively, were used for sensor fabrication.

3.6 Analytical performance of ZrO_2@ZIF-90/GCE for the detection of MP

Under the optimized experimental conditions, DPV curves were utilized to the evaluate analytical performance of the developed ZrO_2@ZIF-90 sensor for MP detection. Fig. 5d displayed that anodic peak current was proportional to the MP concentration (3-200 μmol L^{-1}). The two linear ranges (3-10 μmol L^{-1} and 10-200 μmol L^{-1}) were found (Fig. 5e). The linear equation were Ip (μA) = -0.0865C (μmol L^{-1}) + 0.1542 (R^2 = 0.9935) and Ip (μA) = -0.0301C (μmol L^{-1})-0.5027 (R^2 = 0.9911), corresponding to low concentrations and high concentrations, respectively. The low limit of detection (LOD) was 0.53 μmol L^{-1} (S/N = 3). The ZrO_2@ZIF-90/GCE sensor possessed excellent electrochemical properties and wide linear range for MP detection.

ZrO_2@ZIF-90/GCE was compared with the published sensors for the detection of MP in Table S3. The LOD value of the ZrO_2@ZIF-90/GCE sensor was lower than some previously reported sensors[51-55], being only higher than the CCM/UiO-66 sensor[56]. However, the fabrication process of the ZrO_2@ZIF-90/GCE sensor was facile and bifunctional by comparison with the CCM/UiO-66 sensor. Therefore, the ZrO_2@ZIF-90/GCE sensor provides an effective strategy for MP detection.

3.7 Anti-interference, repeatability and reproducibility of the ZrO_2@ZIF-90/GCE sensor

Anti-interference experiments was carried out further explore the analytical performance of the fabricated sensor by adding various common substances to MP solution. Interfering materials included 100 times higher concentration of inorganic ions (Cl^-, K^+, Na^+, NO_2^-) or a 10 times higher concentration of glucose, malathion, glyphosate, chlorpyrifos, acephate, 4-Nitrobenzoic acid and coexistence of all the above interfering substances (Fig. 5f). Compared with the MP solution without of any interferents, peak currents

showed only small changes in the presence of the interferents (0.96% − 10.32%). Therefore, the anti-interference performance of the ZrO_2@ZIF-90/GCE sensor was acceptable.

To evaluate the repeatability of the ZrO_2@ZIF-90 sensor, six equally modified ZrO_2@ZIF-90/GCE sensors were prepared and used to detect a 150 μmol L^{-1} MP solution. The RSD (relative standard deviation) for peak current measured by the six electrodes was only 1.40%, suggesting excellent repeatability of the developed sensor. The measurement reproducibility was estimated by using a single ZrO_2@ZIF-90/GCE to detect a 150 μmol L^{-1} MP solution. The RSD was 3.31%, indicating that the prepared sensor possessed the desired measurement reproducibility.

3.8 Accuracy and applicability of the ZrO_2@ZIF-90/GCE sensor

Recovery experiments were carried out using MP-spiked apple and pear samples to investigate the applicability and accuracy of ZrO_2@ZIF-90/GCE sensor in real samples. Recoveries ranged from 89.25% to 102.78% with RSDs of 2.35% − 7.06% (Table 1). The results clearly confirmed the accuracy and applicability of ZrO_2@ZIF-90/GCE sensor in foods.

Table 1 Recovery of MP in spiked food samples using the ZrO_2@ZIF-90/GCE sensor (n=3).

Samples	Added level (mg kg^{-1})	Found level by the sensor (mg kg^{-1}, ± SD)	Recovery	RSD
Apple	2.63	2.35 ± 0.06	89.25	2.35
	0.53	0.54 ± 0.04	102.60	6.49
	0.26	0.26 ± 0.02	102.78	7.06
Pear	2.63	2.58 ± 0.08	98.22	3.09
	0.53	0.51± 0.01	95.32	1.41
	0.26	0.24 ± 0.03	99.43	4.15

The concentration of MP in river water and tap water samples were also analyzed using the sensor. MP was not found in tap water samples, whilst the content of MP in river samples was 1.90 mg L^{-1}. The result is explained by tap water having been purified whereas the river was polluted.

4. Conclusion

In summary, a bifunctional ZrO_2@ZIF-90 nanozyme was successfully synthesized for degradation and electrochemical detection of MP. The ZrO_2@ZIF-90 nanozyme possessed efficient phosphohydrolase activity, catalyzing the conversion of MP to *p*-NP. When immobilized on a glassy carbon electrode, ZrO_2@ZIF-90/GCE offered strong signal amplification for MP detection (via oxidation of the in-situ formed *p*-NP). Moreover, the developed analytical method possessed excellent repeatability, reproducibility, two wide linear ranges (3-10 μmol L^{-1} and 10-200 μmol L^{-1}) and outstanding anti-interference properties. The sensitivity and selectivity of the constructed sensor need to be further improved. In the future, on the one hand, the selectivity of the method is achieved by designing the nanozyme that can selectively catalyze the substrate, and on the other hand, the sensitivity of the method is improved by surface modification to further enhance the catalytic activity of the nanozyme. To their credit, the method destroys MP and allows its detection, offering many advantages for food and environmental monitoring.

Acknowledgement

This work was financially supported by the National Natural Science Foundation of China (No. 31972149) and Innovation Capability Improvement Project of Scientific and Technological Small and Medium-sized Enterprises in Shandong Province (No. 2022TSGC2409). GINW acknowledges funding support from the MacDiarmid Institute for Advanced Materials and Nanotechnology and the Dodd-Walls Centre for Photonic and Quantum Technologies.

Declaration of Competing Interest

The authors declare that they have no known competing financial interests or personal relationships that could have appeared to influence the work reported in this paper.

References

[1] L.J. Wang, Y. Sun, Engineering organophosphate hydrolase for enhanced biocatalytic performance: A review, Biochem. Eng. J. 168 (2021) 107945. https://doi.org/10.1016/j.bej.2021.107945.

[2] T. Islamoglu, Z.J. Chen, M.C. Wasson, C.T. Buru, K.O. Kirlikovali, U. Afrin, M.R. Mian, O.K. Farha, Metal-organic frameworks against toxic chemicals, Chem. Rev. 120 (2020) 8130-8160. https://doi.org/10.1021/acs.chemrev.9b00828.

[3] P. Mishra, J. Lee, D. Kumar, R.O. Louro, N. Costa, D. Pathania, S. Kumar, J. Lee, L. Singh, Engineered nanoenzymes with multifunctional properties for next-generation biological and environmental applications, Adv. Funct. 32 (2022) 2108650. https://doi.org/10.1002/adfm.202108650.

[4] S. Kumar, G. Kaushik, M.A. Dar, S. Nimesh, U.J. Lopez-Chuken, J.F. Villarreal-Chiu, Microbial degradation of organophosphate pesticides: a review, Pedosphere 28 (2018) 190-208. https://doi.org/10.1016/s1002-0160(18)60017-7.

[5] G. Andrade, S. Monteiro, J. Francisco, L. Figueiredo, R. Botelho, V. Tornisielo, Liquid chromatography-electrospray ionization tandem mass spectrometry and dynamic multiple reaction monitoring method for determining multiple pesticide residues in tomato, Food Chem. 175 (2015) 57-65. http://doi.org/10.1016/j.foodchem.2014.11.105.

[6] G.K. Sidhu, S. Singh, V. Kumar, D.S. Dhanjal, S. Datta, J. Singh, Toxicity, monitoring and biodegradation of organophosphate pesticides: a review, Crit. Rev. Environ. Sci. Technol. 49 (2019) 1135-1187. http://doi.org/10.1080/10643389.2019.1565554.

[7] Y. Pico, A.H. Alfarhan, D. Barcelo, How recent innovations in gas chromatography-mass spectrometry have improved pesticide residue determination: an alternative technique to be in your radar, TrAC-Trend. Anal. Chem. 122 (2020) 115720. https://doi.org/10.1016/j.trac.2019.115720.

[8] J.J. Yao, Z.X. Wang, L.L. Guo, X.X. Xu, L.Q. Liu, L.G. Xu, S.S. Song, C.L. Xu, H. Kuang, Advances in immunoassays for organophosphorus and pyrethroid pesticides, Trends Analyt. Chem. 131 (2020) 116022. https://doi.org/10.1016/j.trac.2020.116022.

[9] C.S. Pundir, A. Malik, Preety, Bio-sensing of organophosphorus pesticides: A review, Biosens. Bioelectron. 140 (2019) 111348. https://doi.org/10.1016/j.bios.2019.111348.

[10] Q. Zhang, Q. Xu, Y. Guo, X. Sun, X.Y. Wang, Acetylcholinesterase biosensor based on the mesoporous carbon/ferroferric oxide modified electrode for detecting organophosphorus pesticides, RSC Adv. 6 (2016) 24698e24703. https://doi.org/10.1039/C5RA21799G.

[11] J.C. Wei, L.L. Yang, M. Luo, Y.T. Wang, P. Li, Nanozyme-assisted technique for dual mode detection of organophosphorus pesticide, Ecotoxicol. Environ. Saf. 179 (2019) 17-23. https://doi.org/10.1016/j.ecoenv.2019.04.041.

[12] W.P. Yang, X. Yang, L.J. Zhu, H.S. Chu, X.Y. Li, W.T. Xu, Nanozymes: Activity origin, catalytic mechanism, and biological application, Coordin. Chem. Rev. 448 (2021) 214170. https://doi.org/10.1016/j.ccr.2021.214170.

[13] A. Kirchon, L. Feng, H.F. Drake, E.A. Josepha, H.C. Zhou, From fundamentals to applications: a toolbox for robust and multifunctional MOF materials, Chem. Soc. Rev. 47 (2018) 8611-8638. https://doi.org/10.1039/C8CS00688A.

[14] H. Furukawa, K.E. Cordova, M. O'Keeffe, O.M. Yaghi, The chemistry and applications of metal-organic frameworks, Science 341 (2013), 1230444. https://10.1126/science.1230444.

[15] H.C. He, L. Hashemi, M.L. Hu, A. Morsali, The role of the counter-ion in metal-organic frameworks' chemistry and applications, Coordin. Chem. Rev. 376 (2018) 319-347. https://doi.org/10.1016/j.ccr.2018.08.014.

[16] H. Furukawa, N. Ko, Y.B. Go, N. Aratani, S.B. Choi, E. Choi, Yazaydin, A.O., Snurr, R.Q., O'Keeffe, M., Kim, J., Yaghi, O.M., Ultrahigh porosity in metal-organic frameworks, Science 329 (2010) 424-428. https://doi.org/10.1126/science.1192160.

[17] T. Kitao, Y.Y. Zhang, S. Kitagawa, B.Wang, T. Uemura, Hybridization of MOFs and polymers, Chem. Soc. Rev. 46 (2017) 3108-3133. https://doi.org/10.1039/C7CS00041C.

[18] Z.J. Chen, H. Jiang, M. Li, M. O'Keeffe, M. Eddaoudi, Reticular chemistry 3.2: Typical minimal edge-Transitive derived and related nets for the design and synthesis of metal-organic frameworks, Chem. Rev. 120 (2020) 8039-8065. https://doi.org/10.1021/acs.chemrev.9b00648.

[19] X. Huang, S. Zhang, Y.J. Tang, X.Y. Zhang, Y. Bai, H. Pang, Advances in metal-organic framework-based nanozymes and their applications, Coord. Chem. Rev. 449 (2021) 214216. https://doi.org/10.1016/j.ccr.2021.214216.

[20] T. Fu, C.J. Xu, R.R. Guo, C.X. Lin, Y.Y. Huang, Y.H. Tang, H. Wang, Q.F. Zhou, Y.H. Lin, Zeolitic imidazolate framework-90 nanoparticles as nanozymes to mimic organophosphorus hydrolase, ACS Appl. Nano Mater. 4 (2021) 3345-3350. https://doi.org/10.1021/acsanm.1c00540.

[21] D.Y. Tong, Y.L. Zhao, Y.Q. Wang, S.W. Nie, S.T. Xiao, Influence of potential contaminants on I2 and CH3I adsorption onto zeolitic imidazolate frameworks (ZIFs) using GCMC simulations, Comput. Mater. Sci. 229 (2023) 112417. https://doi.org/10.1016/j.commatsci.2023.112417.

[22] L.H. Zhang, Q.W. Wang, Y. Qi, L. Li, S.T. Wang, X.H. Wang, An ultrasensitive sensor based on polyoxometalate and zirconium dioxide nanocomposites hybrids material for simultaneous detection of toxic clenbuterol and ractopamine, Sens. Actuators B Chem. 288 (2019) 347-355. https://doi.org/10.1016/j.snb.2019.03.033.

[23] Q. Dong, SY. Shi, Y.S. Xie, Y.P. Wang, X.Q. Zhang, X.Q. Wang, S.Y. Guo, L.Y. Zhu, G.G. Zhang, D. Xu, 2020. Preparation of mesoporous zirconia ceramic fibers modified by dual surfactants and their phosphate adsorption characteristics, Ceram. Int. 46 (2020) 14019-14029. https://doi.org/10.1016/j.ceramint.2020.02.201.

[24] H.Y. Zhao, B.B. Liu, Y.F. Li, B. Li, H.N. Ma, S. Komarneni, One-pot green hydrothermal synthesis of bio-derived nitrogen-doped carbon sheets embedded with zirconia nanoparticles for electrochemical sensing of methyl parathion, Ceram. Int. 46 (2020) 19713-19722. https://doi.org/10.1016/j.ceramint.2020.04.277.

[25] X.C. Wu, J.H. Wei, C.Y. Wu, G.P. lv, L. Wu, ZrO_2/CeO_2/polyacrylic acid nanocomposites with alkaline phosphatase-like activity for sensing, Spectrochim. Acta A Mol. Biomol. Spectrosc. 263 (2021) 120165. https://doi.org/10.1016/j.saa.2021.120165.

[26] R.Q. Liu, Y.S. Wang, B. Li , B.B. Liu, H.N. Ma, D.D. Li, L. Dong, F. Li, X.L. Chen, X.M. Yin, VXC-72R/ZrO_2/GCE-based electrochemical sensor for the high-sensitivity detection of methyl parathion, Materials 12 (2019) 3637. https://doi.org/10.3390/ma12213637.

[27] Y.Z. Sun, J.C. Wei, J. Zou, Z.H. Cheng, Z.M. Huang, L.Q. Gu, Z.F. Zhong, S.L. Li, Y.T. Wang, P. Li, Electrochemical detection of methyl-paraoxon based on bifunctional cerium oxide nanozyme with catalytic activity and signal amplification effect, J. Pharm. Anal. 11 (2021) 653-660. https://doi.org/10.1016/j.jpha.2020.09.002.

[28] L.H. Qiu, P. Lv, C.L. Zhao, X.Y. Feng, G.Z. Fang , J.F. Liu, S. Wang, Electrochemical detection of organophosphorus pesticides based on amino acids conjugated nanoenzyme modified electrodes, Sens. Actuators B Chem. 286 (2019) 386-393. https://doi.org/10.1016/j.snb.2019.02.007.

[29] J.J. Deng, K. Wang, M. Wang, P. Yu, L.Q. Mao, Mitochondria targeted nanoscale zeolitic imidazole framework-90 for ATP imaging in live cells, J. Am. Chem. Soc. 139 (2017) 5877-5882. https://doi.org/10.1021/jacs.7b01229.

[30] G.Z. Li, Z.H. Si, S. Yang, Y. Zhuang, S.Y. Pang, Y.H. Cui, J. Baeyens, P.Y. Qin, A defects-free ZIF-90/6FDA-Durene membrane based on the hydrogen bonding/covalent bonding interaction for gas separation, J. Membr. Sci. 661 (2022) 120910. https://doi.org/10.1016/j.memsci.2022.120910.

[31] G.W. Zhan, H.C. Zeng, A synthetic protocol for preparation of binary multi-shelled hollow spheres and their enhanced oxidation application, Chem. Mater. 29 (2017) 10104-10112. https://doi.org/10.1021/acs.chemmater.7b03875.

[32] J.J. Chen, J.X. Liu, Y.P. Hu, Z.F.Tian, Y.F. Zhu, Metal-organic framework-coated magnetite nanoparticles for synergistic magnetic hyperthermia and chemotherapy with pH-triggered drug release, Sci. Technol. Adv. Mater. 20 (2019) 1043-1054. https://doi.org/10.1080/14686996.2019.1682467.

[33] L. Vaidya, S. Nadar, V. Rathod, Entrapment of surfactant modified lipase within zeolitic imidazolate framework (ZIF)-8, Int. J. Biol. Macromol. 146 (2020) 678-686. https://doi.org/10.1016/j.ijbiomac.2019.12.164.

[34] J. Zhang, X.Y. Wang, Y.H. Wang, D.D. Wang, Z. Song, C.D. Zhang, H.S. Wang, Colorable zeolitic imidazolate frameworks for colorimetric detection of biomolecules, Anal. Chem. 92 (2020) 12670-12677. https://doi.org/10.1021/acs.analchem.0c02895.

[35] J.Y. Tian, Q. Shao, J.K. Zhao, D. Pan, M.Y. Dong, C.X.C. Jia, T. Ding, T.T. Wu, Z.H. Guo, Microwave solvothermal carboxymethyl chitosan templated synthesis of TiO_2/ZrO_2 composites toward enhanced photocatalytic degradation of Rhodamine B, J. Colloid Interface Sci. 541 (2019) 18-29. https://doi.org/10.1016/j.jcis.2019.01.069.

[36] Q.L. Chen, W.L. Yang, J.J. Zhu, L.C. Fu, D.Y. Li, L.P. Zhou, Enhanced visible light photocatalytic activity of g-C_3N_4 decorated ZrO_2-x nanotubes heterostructure for degradation of tetracycline hydrochloride, J. Hazard. Mater. 384 (2020) 121275. https://doi.org/10.1016/j.jhazmat.2019.121275.

[37] W.L. Xie, F. Wan, Guanidine post-functionalized crystalline ZIF-90 frameworks as a promising recyclable catalyst for the production of biodiesel via soybean oil transesterification. Energy Convers. Manag, 198 (2019) 111922. https://doi.org/10.1016/j.enconman.2019.111922.

[38] T.T. Lin, T. Qin, S.S. Jiang, C.F. Zhang, L. Wang, Anti-inflammatory and anti-biotic drug metronidazole loaded ZIF-90 nanoparticles as a pH responsive drug delivery system for improved pediatric sepsis management. Microb. Pathog, 176 (2022) 105941. https://doi.org/10.1016/j.micpath.2022.105941.

[39] L. Qiu, P. Wang, S.D. Zhang, F.D. Qu, H.C. Guo, R.Y. Zhao, T, Tiju, D. Yao, M.H. Yang, Enhanced, stable, humidity-tolerant xylene sensing using ordered macroporous NiO/ZrO_2 nanocomposites, Sens. Actuators B Chem. 324 (2020) 128648. https://doi.org/10.1016/j.snb.2020.128648.

[40] E. Murugan, Z. Poongan, A new sensitive electrochemical sensor based on $BiVO_4/ZrO_2$@graphene modified GCE for concurrent sensing of acetaminophen, phenylephrine hydrochloride and cytosine in medications and human serum samples, Diam. Relat. Mater. 126 (2022) 209117. https://doi.org/10.1016/j.diamond.2022.109117.

[41] Z.Y. Liu, A.P. Wu, H.J. Yan, D.N. Su, C.X. Jin, H. Guo, L. Wang, C.G. Tian, An effective “precursortransformation” route toward the high-yield synthesis of ZIF-8 tubes, ChemComm. 56 (2020) 2913-2916. https://doi.iog/10.1039/C9CC08724A.

[42] Z.L. Wu, L. Wang, S.X. Chen, X.M. Zhu, Q. Deng, J. Wang, Z.L. Zeng, S.G. Deng, Facile and low-temperature strategy to prepare hollow ZIF-8/CNT polyhedrons as high-performance lithium-sulfur cathodes, Chem. Eng. J. 404 (2021) 126579. https://doi.org/10.1016/j.cej.2020.126579.

[43] Y.F. Sun, G.I.N. Waterhouse, L.H. Xu, X.G. Qiao, Z.X. Xu, Three-dimensional electrochemical sensor with covalent organic framework decorated carbon nanotubes signal amplification for the detection of furazolidone, Sens. Actuators B Chem. 321 (2020) 128501. https://doi.org/10.1016/j.snb.2020.128501.

[44] F.A. Beni, M.N. Shahrak, Alkali metals-promoted capacity of ZIF-8 and ZIF-90 for carbon capturing: a molecular simulation study, Polyhedron 178 (2020) 114338. https://doi.org/10.1016/j.poly.2019.114338.

[45] Y.X. Mao, J. Cheng, H. Guo, Y. Shao, L. Qian, W.J. Yang, Sulfamic acid-modified zeolitic imidazolate framework (ZIF-90) with synergetic Lewis and Brønsted acid sites for microalgal biodiesel production, Fuel 331 (2023) 125795. https://doi.org/10.1016/j.fuel.2022.125795.

[46] H. Anwer, J.W. Park, Synthesis and characterization of a heterojunction $rGO/ZrO_2/Ag_3PO_4$ nanocomposite for degradation of organic contaminants, J. Hazard. Mater. 358 (2018) 416-426. https://doi.org/10.1016/j.jhazmat.2018.07.019.

[47] A.A. Vernekar, T. Das, G. Mugesh, Vacancy-engineered nanoceria: enzyme mimetic hotspots for the degradation of nerve agents, Angew. Chem. Int. Ed. 55 (2016) 1412-1416. https://doi.org/10.1002/anie.201510355.

[48] B. Liu, C.M. Li, G.Q. Zhang, X.S. Yao, S.S.C. Chuang, Z. Li, Oxygen vacancy promoting dimethyl carbonate synthesis from CO_2 and methanol over Zr-doped CeO_2 nanorods, ACS Catal. 8 (2018) 10446-10456. https://doi.org/10.1021/acscatal.8b00415.

[49] M. Pontié, G. Thouand, F. De Nardi, I. Tapsoba, S. Lherbette, Antipassivating electrochemical process of glassy carbon electrode (GCE) dedicated to the oxidation of nitrophenol compounds, Electroanalysis 23 (2011) 1579-1584. https://doi.org/10.1002/elan.201100082.

[50] M. Santhiago, C.S. Henry, L.T. Kubota, Low cost, simple three dimensional electrochemical paper-based analytical device for determination of *p*-nitrophenol, Electrochim. 130 (2014) 771-777. https://doi.org/10.1016/j.electacta.2014.03.109.

[51] H.X. Wu, M.C. Rong, Y. Ma, S.D. Chen, PVP-mediated galvanic replacement growth of AgNPs on copper foil for SERS sensing, Nanomicro. Lett. 15 (2020) 590-594. https://doi.org/10.1049/mnl.2020.0148.

[52] M. Jain, P. Yadav, B. Joshi, A. Joshi, P. Kodgire, Recombinant organophosphorus hydrolase (OPH) expression in E. coli for the effective detection of organophosphate pesticides, Protein Expr. Purif. 186 (2021) 105929. https://doi.org/10.1016/j.pep.2021.105929.

[53] J. Kumar, S.F. D'Souza, An optical microbial biosensor for detection of methyl parathion using Sphingomonas sp immobilized on microplate as a reusable biocomponent, Biosens. Bioelectron. 26 (2010) 1292-1296. https://doi.org/10.1016/j.bios.2010.07.016.

[54] R. Kaur, S. Rana, K. Lalit, P. Singh, K. Kaur, Electrochemical detection of methyl parathion via a novel biosensor tailored on highly biocompatible electrochemically reduced graphene oxide-chitosan-haemoglobin coatings, Biosens. Bioelectron. 167 (2020) 112486. https://doi.org/10.1016/j.bios.2020.112486.

[55] J.N. Nirmala, A. Kumaravel, M. Chandrasekaran, Stearic acid modified glassy carbon electrode for electrochemical sensing of parathion and methyl parathion(Article), J. Appl. Electrochem. 40 (2010) 1721–1727. https://doi.org/10.1007/s10800-010-0125-7.

[56] J. Cao, Z.H. Yang, W.P. Xiong, Y.Y. Zhou, Y.R. Peng, X. Li, C.Y. Zhou, R. Xu, Y. R. Zhang, One-step synthesis of Co-doped UiO-66 nanoparticle with enhanced removal efficiency of tetracycline: Simultaneous adsorption and photocatalysis, Chem. Eng. J. 353 (2018) 126-137. https://doi.org/10.1016/j.cej.2018.07.060.